Quenched and annealed disorder in randomly grafted copolymer melts

Deena M. Patel*
Physics Department, University of California, Santa Barbara, California 93106, USA

Glenn H. Fredrickson†
Departments of Chemical Engineering and Materials, University of California, Santa Barbara, California 93106, USA

(Received 15 July 2003; published 21 November 2003)

A model of randomly grafted *AB* copolymer melts is constructed in which flexible *B* polymer grafts are statistically attached at three possible sites along flexible *A* polymer backbones. An incompressible melt of such molecules is examined theoretically at equilibrium for two situations: (1) the grafting is irreversible so that the chemical disorder associated with the statistical placement of the grafts is *quenched*, and (2) the grafting is reversible so that the disorder is *annealed*. Because of the simplicity of the model, we are able to exactly carry out the two types of disorder averages, yielding effective field theories for the quenched and annealed cases. These field theories are investigated in the mean-field approximation, but without further invoking the usual weak-amplitude random phase approximation. Our results clarify the conditions for which quenched and annealed averages can be interchanged.

DOI: 10.1103/PhysRevE.68.051802 PACS number(s): 82.35.Jk

I. INTRODUCTION

Block and graft copolymers are fascinating materials that can exhibit unusual combinations of properties resulting from their ability to self-assemble into nanostructured morphologies [1]. This so-called microphase separation of copolymers arises from the competing effects of repulsion between dissimilar polymer segments and the intramolecular chemical linkages that hold the blocks or grafts together [2]. Copolymers that are prepared for commercial use are often not pure materials, but represent complex mixtures of molecules with varying block lengths, compositions, overall molecular weight, and architecture. For example, styrenic triblock and starblock copolymers are typically ''contaminated'' with varying amounts of diblock copolymers. Significant concentrations of such diblock impurities can damage the large strain recovery characteristics of thermoplastic elastomers based on these materials [3]. Graft copolymers, which are typically prepared by reactive blending processes, are inherently even more ''architecturally disordered'' since the random placement of reactive grafting sites and the statistical nature of the grafting reactions leads to molecules with large variations in the number and placement of grafts [4].

Despite the prevalence of chemical disorder in commercial copolymer materials, very little is understood from a theoretical standpoint about the ramifications of such disorder on phase behavior, self-assembly, and physical properties. This lack of understanding has become more acute in recent years with the advent of controlled free radical polymerization methods [5]. These techniques have created exciting opportunities for producing new types of block and graft copolymers, including the incorporation of highly functional monomers, but are inherently less ''controlled'' than traditional anionic and cationic polymerization methods.

Over the past decade, there have been a number of theoretical studies of chemical disorder effects on the self-assembly behavior of polymer blends and copolymers [6–19]. Of primary interest to such investigators has been the phase behavior of *AB* random copolymers and *AB* random multiblock copolymers with different statistical models of the sequence distributions of the two types of monomers (blocks). Such studies also have relevance to protein folding phenomena. There have also been a few investigations of *AB* graft copolymers where the locations of the grafting points are random variables [20–24]. Some common themes arise from these studies; specifically, that large amounts of polydispersity can lead to a competition between macrophase separation and microphase separation, delineated in some cases by Lifshitz tricritical points, and that the length scales of the mesophases are strongly temperature dependent, unlike pure block copolymer systems. Nevertheless, there are a number of unsatisfactory features surrounding these theoretical results.

In most chemically disordered heterogeneous polymers, the disorder is *quenched* in that it is locked permanently into the macromolecules by virtue of covalent or other strong bonds. A few systems, such as polyesters capable of transesterification, are exceptions; in these cases the disorder can *anneal* in time by means of breaking and reforming chemical bonds. Theoretically, this difference amounts to averaging the partition function of the system over the random disorder variables in the annealed case and the free energy (or logarithm of the partition function) in the quenched case. Theorists to date have performed such quenched averages only in the limiting case of weak segregation (when the composition variations defining the mesophases are small in amplitude). The replica formalism used in spin glass physics is useful for this purpose [25], but the formalism is only tractable in a weak segregation expansion. In contrast, for some models of annealed disorder it is possible to analytically average the partition function over the disorder variables without limiting

*Electronic address: deena@physics.ucsb.edu
†Electronic address: ghf@mrl.ucsb.edu

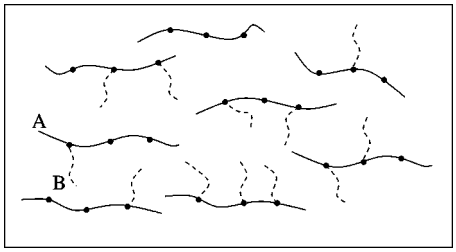

FIG. 1. Randomly grafted copolymer system with three possible graft sites per backbone. All eight possibilities are shown but note that there are only six topologically distinct species.

the applicability of the theory to weakly segregated systems. One major unresolved issue is under what conditions are heterogeneous polymer systems with quenched and annealed disorder different? For example, one might guess that in a very large system with quenched disorder, frustration at some location in a fluid could be relieved by exchanging molecules with more appropriate molecules drawn from the reservoir. An annealed system could achieve the same effect by simply transforming the unhappy molecules at the location into more suitable ones. It is important to understand the relationship between the two types of systems better because if quenched averages can be accurately replaced by (simpler) annealed averages, a much more complete theoretical analysis of the structure and phase behavior of chemically disordered polymer systems would be possible.

In the present paper, we tackle this issue in the context of a very simple model of randomly grafted *AB* copolymers. As shown in Fig. 1, we consider an incompressible melt of flexible polymer chains in which each type *A* backbone contains three sites at which type *B* grafts can be attached. The grafting sites are equally spaced and the probabilities of attachment of the various sites are uniform and uncorrelated. We further assume that the *A* backbones and the *B* grafts are monodisperse. This model, while unrealistic in several aspects, contains the essential physics of a varying number of grafts per molecule (from zero to three) and varying placement of those grafts along the backbone. Because the total number of species can be easily enumerated, it is possible to *exactly* perform both quenched and annealed averages for this model, *independent* of any simplifying assumptions such as weak segregation. As a result, we will be able to investigate in detail the difference in self-assembly behavior between systems containing quenched and annealed disorder. The main focus of this paper is to study whether treating the disorder as annealed reasonably approximates a more realistic system with quenched disorder.

II. MODEL

We consider a melt of n polymers, each comprised of a flexible homopolymer *A* backbone along which flexible grafts of homopolymer *B* are attached. The placement of the *B* grafts is random and varies from polymer to polymer. We shall later specialize to the case where the grafts can be attached at only three equally spaced sites along each *A* backbone, as in Fig. 1, but will begin by discussing a more general case. Starting with a coarse grained picture of Gaussian chains and adding in binary interactions parametrized by a (AB) Flory-Huggins parameter χ and an incompressibility constraint [26], the configurational partition function is

$$Z=\prod_{i=1}^{n}\prod_{j}\int \mathcal{D}[\mathbf{R}_{Ai}]\mathcal{D}[\mathbf{R}_{Bj}]e^{-U_o[\mathbf{R}_A]-U_o[\mathbf{R}_B]} \times\exp\left(-v_0\chi\int d\mathbf{r}\hat{\rho}_A(\mathbf{r})\hat{\rho}_B(\mathbf{r})\right) \times\prod_{\mathbf{r}}\delta(\hat{\rho}_A(\mathbf{r})+\hat{\rho}_B(\mathbf{r})-\rho_0). \quad (1)$$

In this expression the δ functional enforces incompressibility by setting the total microscopic densities of *A* and *B* monomers, $\hat{\rho}_A(\mathbf{r})+\hat{\rho}_B(\mathbf{r})$, at each point in space equal to a constant ρ_0. Monomer (statistical segment) volumes of the two species are assumed equal and given by $v_0=1/\rho_0$. Implicit in the path integrals over the backbone conformations $\mathbf{R}_{Ai}(s)$ and the graft conformations $\mathbf{R}_{Bj}(s)$ are constraints that fix the architecture of each of the n polymers such that one end of each of the *B* grafts is tethered to a fixed place along one of the *A* backbones. We note that our model allows for free (ungrafted) *A* homopolymer, but assumes that there are no ungrafted *B* chains.

The statistical weight associated with the conformations of the Gaussian chain segments is given by e^{-U_o}:

$$U_o[\mathbf{R}_k]=\sum_i \frac{d}{2b^2}\int_0^{N_k}ds\left|\frac{d\mathbf{R}_{ki}(s)}{ds}\right|^2, \quad k=A,B. \quad (2)$$

The statistical segment lengths, given by b, are for simplicity taken to be the same on both the *A* and *B* chain segments. The degrees of polymerization of the *A* and *B* chains are N_A and N_B, respectively, and d is the spatial dimension. The microscopic density operators are given by

$$\hat{\rho}_k(\mathbf{r})=\sum_i \int_0^{N_k}ds\,\delta(\mathbf{r}-\mathbf{R}_{ki}(s)), \quad k=A,B. \quad (3)$$

Following the well-known procedure described, e.g., in a recent review [26], we can transform this partition function from an expression involving path integrals over all polymer conformations to a new expression involving functional integrals over two fields. This is done by performing a Hubbard-Stratonovich transformation to decouple the Flory-Huggins interaction term, which introduces a field $w_-(\mathbf{r})$, and by expressing the incompressibility δ functional in exponential form, which introduces a second field $w_+(\mathbf{r})$. After rescaling all spatial coordinates by the radius of gyration for an ideal *B* chain $\mathbf{R}_{gB}=b\sqrt{N_B/2d}$ and the fields $w_\pm$ by a factor of $1/N_B$, the partition function can be transformed into a form involving functional integrals over the $w_\pm$ fields:

$$Z=\int \mathcal{D}[w_-]\int \mathcal{D}[w_+]e^{-H[w_-,w_+]} \quad (4)$$

in which the effective Hamiltonian $H[w_-,w_+]$ is given by

$$H[w_-,w_+]=\frac{C}{\chi N_B}\int d\mathbf{r}\, w_-^2(\mathbf{r})+C(f_A-f_B)\int d\mathbf{r}\, w_-(\mathbf{r}) - iC\int d\mathbf{r}\, w_+(\mathbf{r})-\sum_i n_i \ln Q_i[w_-,w_+]. \tag{5}$$

In this expression, $C=\rho_o/(N_B/R_{gB}^d)$ is a dimensionless polymer concentration parameter, $f_A=nN_A/\rho_0 V$ is the average volume fraction of A monomers, and $f_B=1-f_A$ is the average volume fraction of B monomers. The last term in Eq. (5) represents a sum over all the different species of polymer architecture, where n_i denotes the number of chains of each species i and Q_i is the partition function for a single polymer with that architecture. So for example, the model copolymer melt shown in Fig. 1 would have a sum over eight terms. In the thermodynamic limit, where the total number of polymers $n=\Sigma_i n_i$ becomes large, the sum can be written as an average

$$n\sum_i \frac{n_i}{n}\ln Q_i = n\langle \ln Q\rangle \tag{6}$$

in which the angular brackets denote an ensemble average over the different polymer architectures.

We model the probability distribution function of the polymer species by assuming there are m uncorrelated, equally spaced sites along each A backbone, each site with a probability p of having a B branch attached. Figure 1 evidently corresponds to the case of $m=3$. The probability of having a polymer of species i which has k grafts at contour locations $\tau_1,\tau_2\ldots,\tau_k$ along the backbone is $p_i=p^k(1-p)^{m-k}$. The partition function associated with it is

$$Q_i[w_A,w_B]=\int \mathcal{D}[\mathbf{R}_A]\prod_{j=1}^{k}\int \mathcal{D}[\mathbf{R}_{Bj}]\delta(\mathbf{R}_{Bj}(0) - \mathbf{R}_A(\tau_j))\exp\Big(-U_0[\mathbf{R}_A]-U_0[\mathbf{R}_{Bj}] - \int ds\, w_A(\mathbf{R}_A(s))-\int ds\, w_B(\mathbf{R}_{Bj}(s))\Big). \tag{7}$$

The chemical potential fields w_A and w_B are complex linear combinations of the w_- and w_+ fields:

$$w_A(\mathbf{r})=-w_-(\mathbf{r})+iw_+(\mathbf{r}),$$
$$w_B(\mathbf{r})=w_-(\mathbf{r})+iw_+(\mathbf{r}). \tag{8}$$

After integrating out the positions of the B monomers, Q_i can be expressed as a path integral over a single space curve (representing the backbone conformation) in an external potential $w_A(\mathbf{r})$ with an additional statistical weight $q_B(\mathbf{r},1)$ at each of the branch points along the backbone. Aside from potential independent prefactors,

$$Q_i[w_A,w_B]=\int \mathcal{D}[\mathbf{R}_A]\exp\Big(-U_0[\mathbf{R}_A]-\int ds\, w_A(\mathbf{R}_A(s))\Big) \times\prod_{j=1}^{k} q_B(\mathbf{R}_A(\tau_j),1), \tag{9}$$

where $q_B(\mathbf{r},s)$ is a propagator for the B grafts that satisfies the following complex diffusion equation [27]:

$$\partial_s q_B(\mathbf{r},s)=\nabla^2 q_B(\mathbf{r},s)-w_B(\mathbf{r})q_B(\mathbf{r},s),\quad 0<s\leqslant 1 \tag{10}$$

subject to the initial condition $q_B(\mathbf{r},0)=1$ for the free end of the graft at $s=0$.

We can complete the integration over the backbone conformations to express Q_i as the volume average of an effective A propagator $q_{Ai}(\mathbf{r},s)$ at $s=1$:

$$Q_i=\frac{1}{V}\int d\mathbf{r}\, q_{Ai}(\mathbf{r},1). \tag{11}$$

The backbone propagator is divided into k+1 segments,

$$q_{Ai}(\mathbf{r},s)=q_{Ai}^{(j)}(\mathbf{r},s)\quad \text{for}\quad \tau_j\leqslant s<\tau_{j+1}\quad j=0,1,\ldots,k,$$
$$\tau_0\equiv 0,\quad \tau_{k+1}\equiv 1, \tag{12}$$

where each segment satisfies the diffusion equation

$$\frac{N_B}{N_A}\partial_s q_{Ai}^{(j)}(\mathbf{r},s)=\nabla^2 q_{Ai}^{(j)}(\mathbf{r},s)-w_A(\mathbf{r})q_{Ai}^{(j)}(\mathbf{r},s) \tag{13}$$

and is subject to the following initial conditions:

$$q_{Ai}^{(j)}(\mathbf{r},\tau_j)=q_{Ai}^{(j-1)}(\mathbf{r},\tau_j)q_B(\mathbf{r},1),\quad j=1,2,\ldots,k$$
$$q_{Ai}^{(0)}(\mathbf{r},0)=1. \tag{14}$$

It proves convenient to also define a backwards propagator $q_{Ai}^{\dagger}(\mathbf{r},s)$ that has branches at $(1-\tau_k),(1-\tau_{k-1}),\ldots,(1-\tau_1)$ and is similarly subdivided as

$$q_{Ai}^{\dagger}(\mathbf{r},s)=q_{Ai}^{\dagger(j)}(\mathbf{r},s)$$
$$\text{for}\ \ (1-\tau_{k-j+1})<s\leqslant(1-\tau_{k-j}),\quad j=0,1,\ldots,k. \tag{15}$$

Each segment of this function also obeys the diffusion equation (13) and is subject to the following initial conditions

$$q_{Ai}^{\dagger(j)}(\mathbf{r},1-\tau_{k-j+1})=q_{Ai}^{\dagger(j-1)}(\mathbf{r},1-\tau_{k-j+1})q_B(\mathbf{r},1),$$
$$j=1,2,\ldots,k,$$
$$q_{Ai}^{\dagger(0)}(\mathbf{r},0)=1. \tag{16}$$

A. Quenched case

In the situation of a quenched distribution of branch sites, we apply the above formalism and make the replacement

$$\sum_i n_i \ln Q_i = n \sum_i p_i \ln Q_i, \tag{17}$$

where the sum on the right hand side is over all species containing any number of branches at the m prescribed sites and runs from 1 to 2^m.

B. Annealed case

In the case of an annealed distribution of branch sites, we can directly average the partition function Z over the disorder. After the Hubbard-Stratonovich transformation, this implies that we can independently average the partition function Q for each chain. Equivalently, the annealed case follows by the approximation

$$\langle \ln Q \rangle \cong \ln \langle Q \rangle \tag{18}$$

in the formulas appropriate for the quenched case.

If there are m uncorrelated grafting sites at positions $\tau_1, \tau_2, \ldots, \tau_m$ along the backbone such that at each site there is a branch with probability p and no branch with probability $1-p$, then the averaged partition function is

$$\langle Q \rangle = \int \mathcal{D}[\mathbf{R}_A] \exp\left(-U_0[\mathbf{R}_A] - \int ds\, w_A(\mathbf{R}_A(s)) \right) \prod_{j=1}^{m} [p q_B(\mathbf{R}_A(\tau_j),1) + 1 - p]. \tag{19}$$

This is similar to the case of a single branched polymer with m branches except that $q_B(\mathbf{r},1)$ is replaced by $p q_B(\mathbf{r},1)+1-p$ at each site. Things are simplified because now we only have one *disorder-averaged propagator* to deal with. As before, we can write

$$\langle Q \rangle = \frac{1}{V} \int d\mathbf{r}\, q(\mathbf{r},1). \tag{20}$$

Breaking $q(\mathbf{r},s)$ up into $m+1$ sections leads to

$$q(\mathbf{r},s) = q^{(j)}(\mathbf{r},s) \quad \text{for} \quad \tau_j \leqslant s < \tau_{j+1}, \quad j = 0,1,\ldots m,$$
$$\tau_0 \equiv 0, \quad \tau_{m+1} \equiv 1. \tag{21}$$

Each section obeys the diffusion equation (13) and has the initial condition

$$q^{(j)}(\mathbf{r},\tau_j) = q^{(j-1)}(\mathbf{r},\tau_j)[p q_B(\mathbf{r},1) + 1 - p],$$
$$j = 1,2,\ldots,m,$$
$$q^{(0)}(\mathbf{r},0) = 1. \tag{22}$$

III. SELF-CONSISTENT MEAN-FIELD THEORY

In the limit of large C, which is achieved at high concentration of polymers or high molecular weight, the functional integrals in Eq. (4) are dominated by the saddle point field configurations. Assuming that this situation holds, the saddle point equations for the fields correspond to

$$\frac{1}{C} \frac{\delta H}{\delta w_A(\mathbf{r})} = \frac{1}{2\chi N_B} [w_A(\mathbf{r}) - w_B(\mathbf{r})] + \phi_A(\mathbf{r}) - f_A = 0, \tag{23}$$

$$\frac{1}{C} \frac{\delta H}{\delta w_B(\mathbf{r})} = \frac{1}{2\chi N_B} [w_B(\mathbf{r}) - w_A(\mathbf{r})] + \phi_B(\mathbf{r}) - f_B = 0, \tag{24}$$

where

$$\phi_k(\mathbf{r}) = -\frac{n}{C} \frac{\delta \langle \ln Q \rangle}{\delta w_k(\mathbf{r})}, \quad k = A,B \tag{25}$$

represents the local volume fraction of type k monomers. These nonlinear equations for the ''self-consistent'' potential fields w_A, w_B are the equations of self-consistent mean-field theory (SCMFT) [28–30].

$\phi_k(\mathbf{r})$ can be decomposed into a sum of terms $\phi_{ki}(\mathbf{r})$, which represent the contribution to the local volume fraction of type k monomers from polymers of species i:

$$\phi_k(\mathbf{r}) = \sum_i \phi_{ki}(\mathbf{r}) = -\frac{n}{C} \sum_i p_i \frac{\delta \ln Q_i}{\delta w_k(\mathbf{r})}. \tag{26}$$

Each term in this sum can be written in terms of the single-polymer propagators [27]

$$\phi_{Ai}(\mathbf{r}) = \frac{f_A p_i}{Q_i} \int_0^1 ds\, q_{Ai}(\mathbf{r},s) q^\dagger_{Ai}(\mathbf{r},1-s), \tag{27}$$

$$\phi_{Bi}(\mathbf{r}) = \frac{f_B p_i}{Q_i} \sum_j \int_0^1 ds\, q_B(\mathbf{r},s) q^\dagger_{Bij}(\mathbf{r},1-s). \tag{28}$$

$q^\dagger_{Bij}(\mathbf{r},s)$ is the propagator of the jth B chain of the ith polymer species. It satisfies Eq. (10) and starts on the end of the B chain tethered to the backbone. It is therefore subject to the initial condition

$$q^\dagger_{Bij}(\mathbf{r},0) = q^{(j-1)}_{Ai}(\mathbf{r},\tau_j) q^\dagger_{Ai}(\mathbf{r},1-\tau_j). \tag{29}$$

These equations complete the description of SCMFT for the case of a random graft copolymer melt with *quenched* disorder.

In the *annealed* case, the formulas are slightly different. The local volume fraction of species k monomers is given by

$$\phi_k(\mathbf{r}) = -\frac{n}{C} \frac{\delta \ln \langle Q \rangle}{\delta w_k(\mathbf{r})} \tag{30}$$

and can also be written as a sum of the volume fractions of the different polymer species,

$$\phi_k(\mathbf{r}) = \sum_i \phi_{ki}(\mathbf{r}) = -\frac{n}{C} \frac{1}{\langle Q \rangle} \sum_i p_i \frac{\delta Q_i}{\delta w_k(\mathbf{r})}. \tag{31}$$

Again, these species volume fractions can be expressed in terms of single-chain propagators, but this time normalized with the averaged partition function $\langle Q \rangle$:

$$\phi_{Ai}(\mathbf{r}) = \frac{f_A p_i}{\langle Q \rangle} \int_0^1 ds\, q_{Ai}(\mathbf{r},s) q_{Ai}^{\dagger}(\mathbf{r},1-s), \tag{32}$$

$$\phi_{Bi}(\mathbf{r}) = \frac{f_B p_i}{\langle Q \rangle} \sum_j \int_0^1 ds\, q_B(\mathbf{r},s) q_{Bij}^{\dagger}(\mathbf{r},1-s). \tag{33}$$

It is possible to show from Eqs. (27) and (28) for the quenched volume fractions that $(1/V)\int d\mathbf{r}\phi_{ki}(\mathbf{r}) = f_k p_i$, indicating that the average volume fraction of polymers from each species is fixed irrespective of the saddle point value of the w fields. This is not necessarily true for the annealed ensembles where the free energy may be lowered by changing the average number of polymers in each species. However, the overall A and B volume fractions $(1/V)\int d\mathbf{r}\phi_k(\mathbf{r}) = f_k$ are fixed in both situations, quenched and annealed.

Alternatively for the annealed case, instead of keeping track of all the different propagators for each realization of the disorder, we can simply use the averaged propagator (20) to calculate the total A and B monomer densities:

$$\phi_A(\mathbf{r}) = \frac{f_A}{\langle Q \rangle} \int_0^1 ds\, q(\mathbf{r},s) q^{\dagger}(\mathbf{r},1-s), \tag{34}$$

$$\phi_B(\mathbf{r}) = \frac{f_B}{\langle Q \rangle} \sum_j \int_0^1 ds\, q_{Bj}^{\dagger}(\mathbf{r},s) q_B(\mathbf{r},1-s). \tag{35}$$

In this case, the backwards propagator $q_{Bj}^{\dagger}(\mathbf{r},s)$ starts from the end of the B chain tethered to the backbone at site j. This object satisfies the diffusion equation (10) with the initial condition

$$q_{Bj}^{\dagger}(\mathbf{r},0) = q^{(j-1)}(\mathbf{r},\tau_j) q^{\dagger}(\mathbf{r},1-\tau_j). \tag{36}$$

It is important to note that Eqs. (34) and (35) are simpler and less computationally demanding to use for the annealed case than Eqs. (32) and (33). However, Eqs. (34) and (35) do not contain information on the monomer densities of the individual chain species, only on the overall monomer densities irrespective of what type of polymer it is attached to. Nevertheless, they can provide a considerable cost savings in situations that do not demand such species accounting.

IV. NUMERICAL METHODS

In order to find saddle points numerically and thereby implement SCMFT, we use a relaxation method

$$\partial_t w_-(\mathbf{r},t) = -\lambda \frac{\delta H}{\delta w_-(\mathbf{r},t)}, \quad \partial_t w_+(\mathbf{r},t) = -\lambda \frac{\delta H}{\delta w_+(\mathbf{r},t)}, \tag{37}$$

the equilibrium values of which correspond to the saddle point equations. Here "time" t is a continuous parameter describing the progress of field iterations to approach a saddle point and λ is an arbitrary relaxational parameter. Since the saddle points can be anywhere in the complex plane, w_- and w_+ have real and imaginary parts, so the complex equations (37) are actually a set of four real equations. It turns out that the saddle point value of w_- is purely real and w_+ is purely imaginary [26], so w_A and w_B are both real and the number of real equations is reduced to two.

Writing Eqs. (37) in terms of the real $w_A(\mathbf{r})$ and $w_B(\mathbf{r})$ fields and using an explicit (forward Euler) time discretization leads to

$$w_A^{j+1}(\mathbf{r}) = w_A^j(\mathbf{r}) + 2\lambda \left[\frac{1}{2\chi N_B} [w_B^j(\mathbf{r}) - w_A^j(\mathbf{r})] + \phi_B^j(\mathbf{r}) - f_B \right],$$

$$w_B^{j+1}(\mathbf{r}) = w_B^j(\mathbf{r}) + 2\lambda \left[\frac{-1}{2\chi N_B} [w_B^j(\mathbf{r}) - w_A^j(\mathbf{r})] + \phi_A^j(\mathbf{r}) - f_A \right]. \tag{38}$$

Superscripts in these expressions refer to the time step. Our basic procedure is as follows. We start with some initial configuration for the w_k fields, either random or containing the symmetry of a particular phase. These are used to determine the propagators by solving the diffusion equations (10) and (13). The propagators are used to find ϕ_A and ϕ_B from Eqs. (27) and (28) for the quenched case or Eqs. (32) and (33) for the annealed case. We then update w_A and w_B according to Eq. (38), the updated fields are used as the new initial fields, and the procedure is repeated until the fields attain equilibrium values. At every iteration the monomer volume fraction of each species is calculated so it is easy to monitor the density configurations. In the case of annealed disorder, a considerable computational savings is obtained by restricting attention to the averaged propagators and substituting Eqs. (34) and (35) for Eqs. (32) and (33) up *until the last field iteration*. At this point, Eqs. (32) and (33) are employed one more time so that the individual species densities may be accessed.

We solve the various diffusion equations using a pseudospectral algorithm developed by Tzeremes *et al.* [31], which is referred to as a *split-step Fourier* algorithm. The integrals in equations such as Eqs. (27), (28), (32), and (33) are approximated using Simpson's rule, which is no more expensive computationally than a midpoint approximation, but has a truncation error that goes like Δs^4 and is consistent with the accuracy of the split-step Fourier algorithm.

All simulations were done in two dimensions on a 64×64 lattice with periodic boundary conditions. Contour step sizes for the A backbone and B grafts were set at $\Delta s_A = 0.0125$ and $\Delta s_B = 0.025$, respectively. In all the results presented, we observed no noticeable changes upon further reducing these contour step sizes.

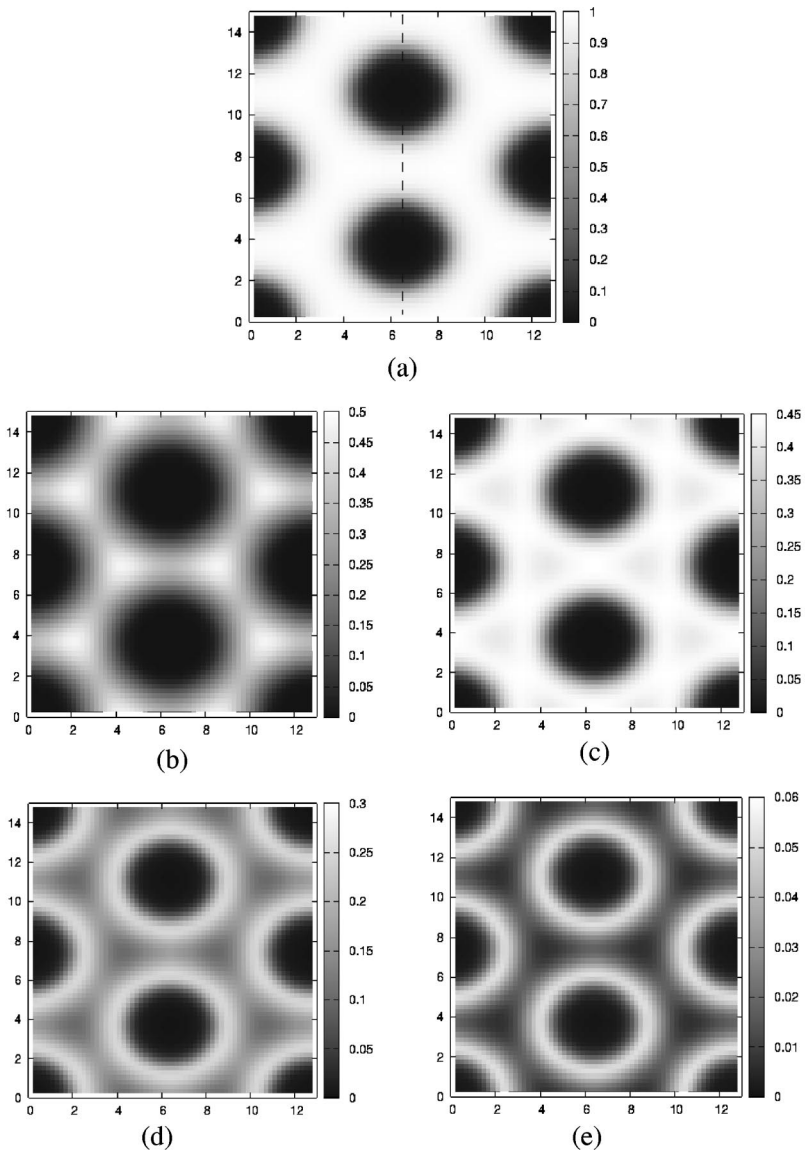

FIG. 2. Density plot of A monomers for the quenched system with $p=0.333$, $N_A/N_B=2$, $\chi N_B=10$. (a) Density of A monomers. (b) Density of A monomers from polymers with zero branches, (c) one branch, (d) two branches, and (e) three branches. Distances are in units of R_{gB}. Box size is 12.6×14.78.

V. RESULTS AND DISCUSSION

A. Quenched versus annealed disorder

For the purposes of comparing the behavior of the quenched and annealed ensembles we restrict attention to the case of $m=3$ and thereby limit the possible polymer architectures to those with zero, one, two, or three branches. Each polymer backbone has three possible graft points at $s = 1/4$, 1/2, and 3/4. At each of these sites a B chain is attached with probability p. This model results in the eight types of polymers, as shown in Fig. 1. Within the course of our simulations, we monitored the densities of A and B segments attached to polymers with zero, one, two, and three branches.

One set of simulations for the *quenched* model was performed with $p=0.333$ (average of one branch per polymer) and with the backbone twice as long as a branch $N_A/N_B=2$. This sets the average volume fractions of A and B monomers at $f_A=0.667$ and $f_B=0.333$, respectively. We started with random initial conditions in a periodic cell of area $(25.6R_{gB})^2$. For $\chi N_B \gtrsim 5$, i.e., above the order-disorder transition (ODT), we observed a microphase segregated phase with hexagonal packing where the B monomers (branches) form the insides of the circular aggregates. Close to the ODT, a defect-free hexagonal phase forms easily (at $\chi N_B=5$ it takes around 5000 time steps using a relaxation parameter of $\lambda=0.5$). At higher χN_B, the interfaces are steeper and longer runs are required to anneal out defects from simulations that are started from random initial conditions.

In order to look more closely at the structure of the A-B interfaces, we chose a box size to capture one cell of the hexagonal lattice and seeded it using an initial condition with

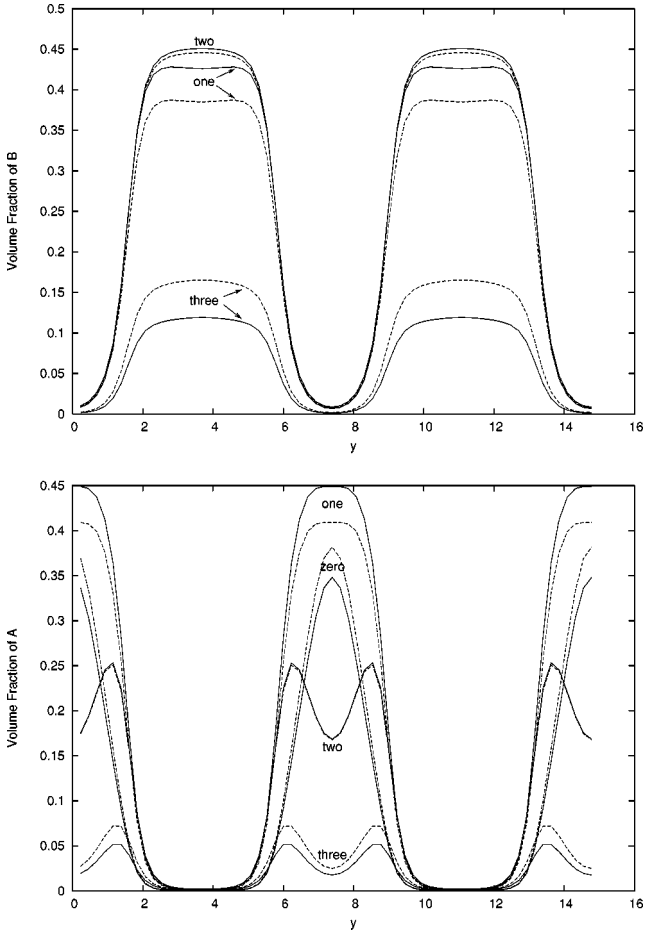

FIG. 3. Simulation results for quenched (solid lines) and annealed (dashed lines) systems with the parameters of Fig. 2. Volume fractions of *A* and *B* monomers from polymers with zero, one, two, and three branches are taken from a slice through the center of the circles as shown by the dashed line in Fig. 2(a). The overall volume fractions (not shown) of *A* or *B* monomers are indistinguishable for the quenched and annealed systems.

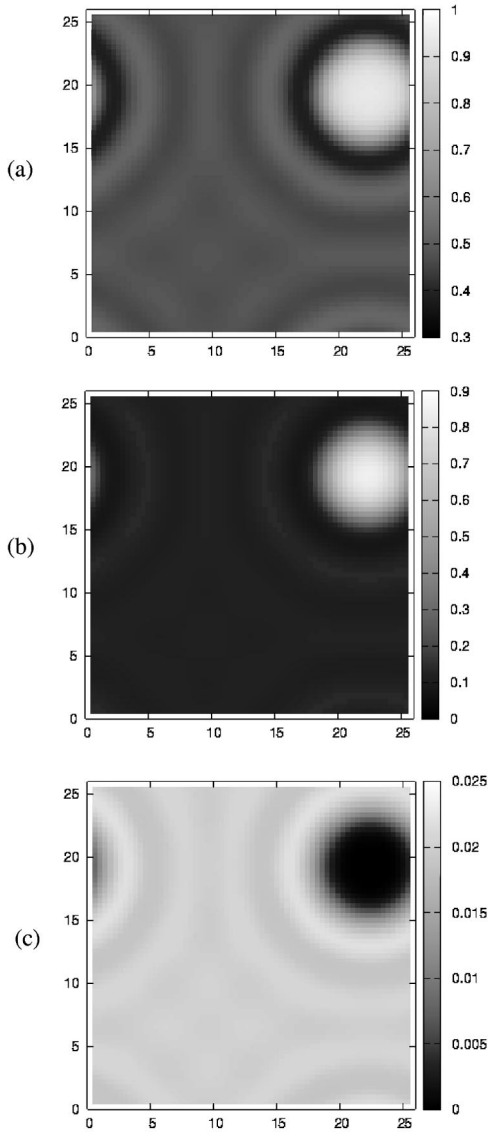

FIG. 4. Simulations of copolymers with quenched disorder and parameters $p=0.333$, $N_A/N_B=1$, $\chi N_B=5.9$. (a) Total volume fraction of *A* monomers. (b) Volume fraction of *A* monomers from zero branched copolymers and (c) three branched copolymers. Box size is $25.6R_{gB}\times 25.6R_{gB}$.

hexagonal symmetry. The box size was determined by fixing the number of lattice points to 64×64 and varying the lattice spacing in the *x* and *y* directions to find a minimum free energy per unit volume (H/V). Figure 2(a) shows the total volume fraction of *A* (backbone) monomers for the quenched system. Figure 2(b) shows the contribution to the *A* volume fraction from the polymers with no branches. Figures 2(c), (d), and (e) correspond to the *A* volume fraction contributions from one, two, and three branched polymers, respectively. The zero branched polymers (*A* homopolymers) tend to be concentrated in the *A*-rich region, particularly at threefold vertices delineating adjacent Wigner-Seitz cells. In contrast, polymers with two and three grafts tend to be more strongly localized along the *A*-*B* interfaces. This allows their branches to more easily stretch into the discrete *B*-rich domains.

Simulations of the annealed model were very similar; the ODT occurred at roughly the same χN_B and the hexagonal microphase morphology was also observed with the same periodicity. To compare them in detail, we have plotted in Fig. 3(a) the volume fraction profiles of a one-dimensional slice cutting through the center of the circles as indicated by the dashed line in Fig. 2(a). Interestingly, the *total volume fraction of A monomers is indistinguishable* for the quenched and annealed cases, but the partial volume fractions of the different species differ as is shown in Fig. 3(a). Figure 3(b) shows the analogous plot for the *B* monomers. There are more zero and three branched polymers in the annealed system than in the quenched system and less one and two branched polymers. This can be understood by realizing that in the annealed system, a one branched polymer situated in the *A* region and a two branched polymer located in a *B* domain can lower their overall energy by exchanging a branch (and thereby annihilating) to create a pair of zero branch and three branch polymers. The global population of

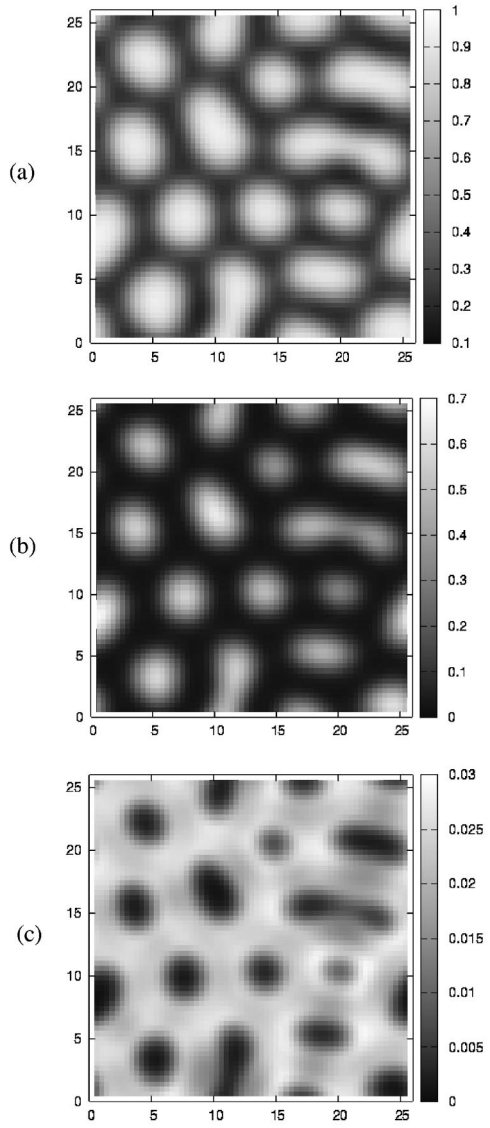

FIG. 5. Simulations of copolymers with quenched disorder and parameters $p=0.333$, $N_A/N_B=1$, $\chi N_B=7.0$ (a) Total volume fraction of *A* monomers. (b) Volume fraction of *A* monomers from zero branched and (c) three branched copolymers. Box size is $25.6R_{gB}\times 25.6R_{gB}$.

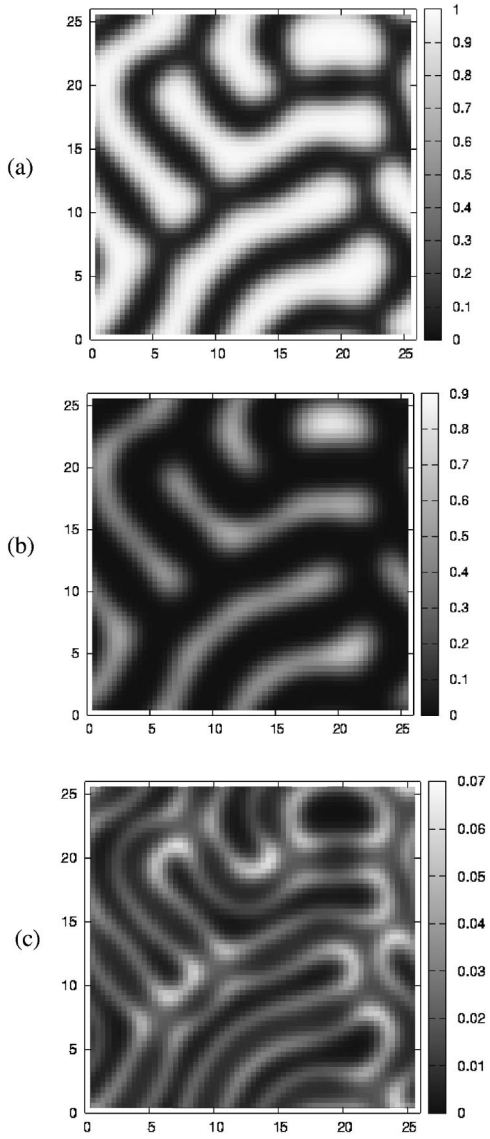

FIG. 6. Simulations of copolymers with quenched disorder and parameters $p=0.333$, $N_A/N_B=1$, $\chi N_B=10.0$. (a) Total volume fraction of *A* monomers. (b) Volume fraction of *A* monomers from zero branched and (c) three branched copolymers. Box size is $25.6R_{gB}\times 25.6R_{gB}$.

branches and overall composition is not affected by this exchange, but the individual species densities clearly respond to the local thermodynamic forces that act upon them.

The observation that the *overall* volume fraction patterns and corresponding saddle point potential fields are indistinguishable between the quenched and annealed cases lends strong support to the naive expectation that the free energies and thermodynamic properties of block and graft copolymers with quenched and annealed disorder should be identical in the thermodynamic limit. We caution the reader, however, that this conclusion is likely restricted to microphase separated states, and not to the ''glassy states'' that have been postulated to exist in certain random heteropolymer models [19,15]. It is also important to note that certain properties or measurements may also be sensitive to particular polymer species components, in which case differences between annealed (living) and quenched systems can be observed.

B. Macrophase and microphase separation

A very different phase behavior was found in simulations when we changed the block length ratios to $N_A/N_B=1$ and kept $p=0.333$. This case of longer grafts is compositionally symmetric with $f_A=f_B=1/2$. Figures 4 –6 show this system with *quenched disorder* at various χN_B parameters. These were started with random initial fields and in a simulation cell of area $25.6R_{gB}\times 25.6R_{gB}$. The system exhibits *macrophase separation* at $\chi N_B=5.9$ as shown in Fig. 8. There is a region of nearly pure *A* monomers and a region that contains a mixture of *A* and *B*. From the species volume fractions, we see that the *A*-rich domain is predominantly *A* ho-

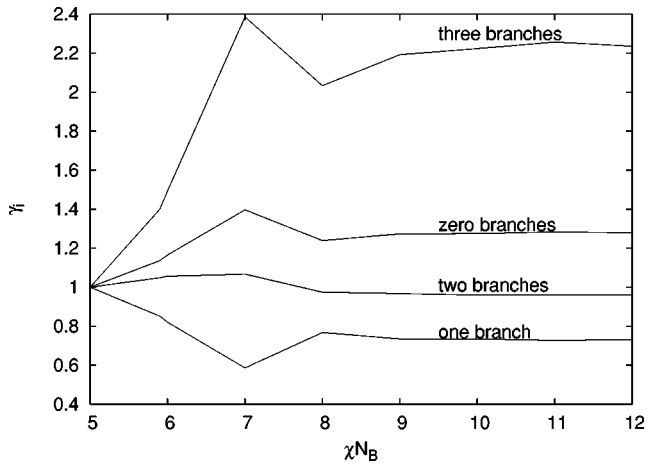

FIG. 7. γ_i vs χN_B for the annealed system with $p=0.333$, $N_A/N_B=1$. The quenched system corresponds to $\gamma_i=1$.

mopolymer (zero branched polymers), while the mixed domain contains the other species. At a slightly higher segregation strength of $\chi N_B=7.0$, depicted in Fig. 5, there is a transition to a *microphase* morphology with the *A* monomers forming the insides of the circular domains. Even after very long runs (100 000 time steps using $\lambda=0.5$) these do not form a defect-free hexagonal array, although starting the simulations with a hexagonal ''seed'' structure does produce an ordered array with lower energy. At even higher $\chi N_B=10$, shown in Fig. 6, we observe a transition to a lamellar microphase structure. Defects are prevalent here as well and indicate the existence of metastable states, since the perfectly ordered lamellar structure has lower free energy.

The annealed case (not shown) follows a similar pattern to that just described, but with the change from macrophase to microphase and hexagonal to lamellar occurring at slightly different values of χN_B. For instance, the $\chi N_B=7$ case shown in Fig. 5 reverts to macrophase separation when the disorder is annealed. For larger values of the segregation strength, we have also observed that the period of the lamellar phase is slightly larger for the annealed system than the quenched. We determined this by seeding the systems with a periodic function (cosine) of period equal to the length of a side of the simulation cell and then varying this length to minimize the free energy per unit volume.

These discrepancies in phase behavior are due to the different amounts of the individual species in the quenched and annealed systems. As previously stated, the average volume fractions of each species for the quenched system are fixed at $(1/V)\int d\mathbf{r}\phi_{Ai}^{(quenched)}(\mathbf{r})=f_A p_i$ while the average volume fractions for the annealed system may deviate from these values. If we fix the average volume fractions to be the same, by adjusting the p_i's, then it is straightforward to show that, at the mean-field level, the two theories are the same. In other words the annealed system with some given value of p_i is the same as a quenched system with $p_i'=(1/f_A V)\int d\mathbf{r}\phi_{Ai}^{(annealed)}(\mathbf{r})$. However p_i' may not correspond to the probability distribution $p^k(1-p)^{m-k}$ described in our model for a polymer with *k* branches and *m* sites. In Fig. 7 we plot the ratio

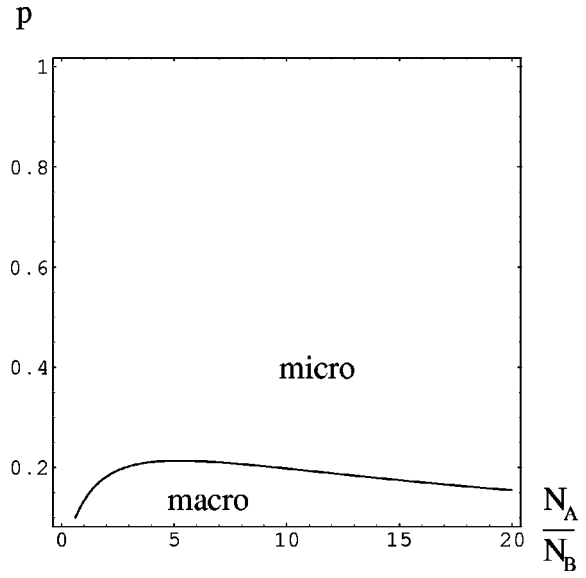

FIG. 8. Phase diagram indicating regions where the disordered phase is unstable to macrophase or microphase separation according to the RPA.

$$\gamma_i=\frac{\frac{1}{V}\int dr\,\phi_{Ai}}{f_A p_i}$$

for the zero, one, two, and three branched volume fractions at different values of χN_B using the annealed system with the same composition as the systems shown in Figs. 4–6. At $\chi N_B=5$ both the quenched and annealed ensembles are in the homogeneous disordered phase and are indistinguishable. Evidently the largest deviation occurs at $\chi N_B=7$ where the annealed system shows macrophase separation and the quenched shows microphase separation.

When the grafting probability was increased to $p=0.667$, or when the length of the backbone was increased relative to the branches to a value of $N_A/N_B=2$, we did not observe macrophase separation for any value of χN_B. Foster *et al.* [24] performed a random phase approximation (RPA) calculation on a closely related model to determine the parameter range in which the homogeneous disordered phase was unstable to macrophase or microphase separation. In this approximation, where the free energy is expanded to quadratic order in the *w* fields, there is no distinction between the quenched and annealed ensembles. Figure 8 shows these stability results for the present case of $m=3$ where there are at most three branches per backbone.

According to this phase diagram, systems with grafting probabilities above $p\approx 0.25$ should not be subject to macrophase separation. However we observe macrophase separation in our simulations for grafting probabilities as high as $p=0.5$. Since our results do not involve any approximations beyond the mean-field approximation, this discrepancy reveals the limitations of the RPA. In particular, our numerical calculations do not make assumptions that the density and potential fields are either small in amplitude or slowly varying in space.

VI. CONCLUDING REMARKS

We have constructed a simple, yet reasonably realistic, field theory model of randomly grafted copolymer melts that has permitted a detailed comparison between systems where the disorder is quenched and systems where it is annealed. We have carried out simulations of the field theory for these two cases by invoking the mean-field approximation (SCMFT). In qualitative terms, quenched and annealed systems are quite similar and under most circumstances that we can foresee, it should be permissible to approximate quenched averages by computationally more efficient annealed averages. Specifically, we have observed that under conditions where well-formed mesophases are obtained, the overall volume fraction profiles and free energies of quenched and annealed systems are very similar. Nevertheless, the distributions of individual copolymer species within such mesophases can be quite different in a system where the chemical disorder is fixed in the molecules (quenched) than in a ''living'' system where polymers can change their compositions or architectures (annealed).

It was interesting that when we performed simulations closer to the ODT where macrophase separation was observed, larger differences (in total volume fractions and locations of phase boundaries) between quenched and annealed systems were detected. In part, this may reflect the finite size of our simulations, but the discrepancies appear too large and insensitive to numerical refinement for this to be the only explanation. It would seem that the ability of annealed systems to respond to local thermodynamic forces by adjusting molecular bonding can produce genuinely different equilibrium states of self-assembly than can be obtained in quenched systems. Thus, it is our view that the naive picture of equivalence of quenched and annealed systems in the thermodynamic limit does not strictly hold. Finally, we note that any discrepancies between quenched and annealed systems in these regions of the phase diagram will undoubtedly be sensitive to fluctuation corrections not included in our SCMFT simulations.

ACKNOWLEDGMENTS

This work was supported by the National Science Foundation under Grant No. DMR-0312097. Use of the UCSB-MRL Central Computing Facilities supported by the NSF is also gratefully acknowledged.

[1] F.S. Bates and G.H. Fredrickson, Phys. Today **52**, 32 (1999).
[2] L. Leibler, Macromolecules **13**, 1602 (1980).
[3] *Thermoplastic Elastomers*, 2nd ed., edited by G. Holden, N. R. Legge, R. P. Quirk, and H. E. Schroeder, (Hanser/Gardner, Cincinnati, OH, 1996).
[4] H. Pernot, M. Baumert, F. Court, and L. Leibler, Nat. Mater. **1**, 54 (2002).
[5] M. Kamigaito, T. Ando, and M. Sawamoto, Chem. Rev. (Washington, D.C.) **101**, 3689 (2001).
[6] A.V. Dobrynin and L. Leibler, Europhys. Lett. **36**, 283 (1996).
[7] A.V. Dobrynin and L. Leibler, Macromolecules **30**, 4756 (1997).
[8] A.N. Semenov, J. Phys. II **7**, 1489 (1997).
[9] A.N. Semenov and A.E. Likhtman, Macromolecules **31**, 9058 (1998).
[10] A.N. Semenov, Eur. Phys. J. B **10**, 497 (1999).
[11] A.V. Subbotin and A.N. Semenov, Eur. Phys. J. A **7**, 49 (2002).
[12] G.H. Fredrickson and S.T. Milner, Phys. Rev. Lett. **67**, 835 (1991).
[13] G.H. Fredrickson, S.T. Milner, and L. Leibler, Macromolecules **25**, 6341 (1992).
[14] E.I. Shakhnovich and A.M. Gutin, J. Phys. (Paris) **50**, 1843 (1989).
[15] C.D. Sfatos, A.M. Gutin, and E.I. Shakhnovich, Nuovo Cimento D **16**, 879 (1994).
[16] A.M. Gutin, C.D. Sfatos, and E.I. Shakhnovich, J. Phys. A **27**, 7957 (1994).
[17] C.D. Sfatos and E. I Shakhnovich, Phys. Rep. **288**, 77 (1997).
[18] C.D. Sfatos, A.M. Gutin, and E.I. Shakhnovich, Phys. Rev. E **48**, 465 (1993).
[19] A.K. Chakraborty, E.I. Shakhnovich, and V.S. Pande, J. Chem. Phys. **108**, 1683 (1998).
[20] S. Qi, A.K. Chakraborty, and N.P. Balsara, J. Chem. Phys. **115**, 3387 (2001).
[21] S. Qi *et al.*, Phys. Rev. Lett. **82**, 2896 (1999).
[22] S. Qi and A.K. Chakraborty, J. Chem. Phys. **115**, 3401 (2001).
[23] A. Shinozaki, D. Jasnow, and A. Balazs, Macromolecules **27**, 2496 (1994).
[24] D.P. Foster, D. Jasnow, and A. Balazs, Macromolecules **28**, 3450 (1995).
[25] M. Mezard, G. Parisi, and M. A. Virasoro, *Spin Glass Theory and Beyond*, Lecture Notes in Physics Vol. 9 (World Scientific, Teaneck, NJ, 1987).
[26] G.H. Fredrickson, V. Ganesan, and F. Drolet, Macromolecules **35**, 16 (2002).
[27] K. Freed, Adv. Chem. Phys. **22**, 1 (1972).
[28] F. Schmid, J. Phys.: Condens. Matter **10**, 8105 (1998).
[29] M.W. Matsen and M. Schick, Phys. Rev. Lett. **72**, 2660 (1994).
[30] M.W. Matsen and M. Schick, Curr. Opin. Colloid Interface Sci. **1**, 329 (1996).
[31] G. Tzeremes, K.O. Rasmussen, T. Lookman, and A. Saxena, Phys. Rev. E **65**, 041806 (2002).